[1] Thomas, A. K., Abraham, K., Thomas, J., & Saban, K. V. (2017). Electrical and dielectric behaviour of $Na_{0.5}La_{0.25}Sm_{0.25}Cu_3Ti_4O_{12}$ ceramics investigated by impedance and modulus spectroscopy. *Journal of Asian Ceramic Societies*, **5**(1), 56-61.

[2] Gavrilyachenko, V. G., Kabirov, Y. V., Panchenko, E. M., Sitalo, E. I., Gavrilyachenko, T. V., Milov, E. V., & Lyanguzov, N. V. (2013). Specific features of the dielectric spectrum of $CaCu_3Ti_4O_{12}$ in the low-frequency range. *Physics of the Solid State*, **55**(8), 1651-1654.

[3] Jesurani, S., Kanagesan, S., Velmurugan, R., Thirupathi, C., Sivakumar, M., & Kalaivani, T. (2011). Nanoparticles of the giant dielectric material, calcium copper titanate from a sol–gel technique. *Materials Letters*, **65**(21-22), 3305-3308.

[4] Schmidt, R., Stennett, M. C., Hyatt, N. C., Pokorny, J., Prado-Gonjal, J., Li, M., & Sinclair, D. C. (2012). Effects of sintering temperature on the internal barrier layer capacitor (IBLC) structure in $CaCu_3Ti_4O_{12}$ (CCTO) ceramics. *Journal of the European Ceramic Society*, **32**(12), 3313-3323.

[5] Aliabadi, T. N., & Alizadeh, P. (2019). Microstructure and dielectric properties of CCTO glass-ceramic prepared by the melt-quenching method. *Ceramics International*, **45**(15), 19316-19322.

[6] Riquet, G., Marinel, S., Bréard, Y., & Harnois, C. (2019). Sintering mechanism and grain growth in $CaCu_3Ti_4O_{12}$ ceramics. *Ceramics International*, **45**(7), 9185-9191.

[7] Kim, B. K., Lee, H. S., Lee, J. W., Lee, S. E., & Cho, Y. S. (2010). Dielectric and Grain-Boundary Characteristics of Hot Pressed $CaCu_3Ti_4O_{12}$. *Journal of the American Ceramic Society*, **93**(9), 2419-2422.

[8] Thongbai, P., Putasaeng, B., Yamwong, T., & Maensiri, S. (2012). Modified giant dielectric properties of samarium doped $CaCu_3Ti_4O_{12}$ ceramics. *Materials Research Bulletin*, **47**(9), 2257-2263.

[9] Fan, J., Leng, S., Cao, Z., He, W., Gao, Y., Liu, J., & Li, G. (2019). Colossal permittivity of Sb and Ga co-doped rutile TiO_2 ceramics. *Ceramics International*, **45**(1), 1001-1010.

[10] Li, M., Sinclair, D. C., & West, A. R. (2011). Extrinsic origins of the apparent relaxorlike behavior in $CaCu_3Ti_4O_{12}$ ceramics at high temperatures: a cautionary tale. *Journal of Applied Physics*, **109**(8), 084106.

[11] Singh, L., Rai, U. S., & Mandal, K. D. (2012). Influence of Zn doping on microstructures and dielectric properties in $CaCu_3Ti_4O_{12}$ ceramic synthesized by semi-wet route. *Advances in Applied Ceramics*, **111**(7), 374-380.

[12] Senda, S., Rhouma, S., Torkani, E., Megriche, A., & Autret, C. (2017). Effect of nickel substitution on electrical and microstructural properties of $CaCu_3Ti_4O_{12}$ ceramic. *Journal of Alloys and Compounds*, **698**, 152-158.

[13] Kim, K. M., Lee, J. H., Lee, K. M., Kim, D. Y., Riu, D. H., & Lee, S. B. (2008). Microstructural evolution and dielectric properties of Cu-deficient and Cu-excess $CaCu_3Ti_4O_{12}$ ceramics. *Materials Research Bulletin*, **43**(2), 284-291.

[14] Amaral, F., Valente, M. A., & Costa, L. C. (2010). Dielectric properties of $CaCu_3Ti_4O_{12}$ (CCTO) doped with GeO_2. *Journal of non-crystalline solids*, **356**(11-17), 822-827.

[15] Sun, X., Wang, C., Wang, G., Lei, C., Li, T., & Liu, L. (2013). Low-Temperature Dielectric Relaxations Associated with Mixed-Valent Structure in $Na_{0.5}Bi_{0.5}Cu_3Ti_4O_{12}$. *Journal of the American Ceramic Society*, **96**(5), 1497-1503.

[16] Sun, X., Wang, C., Wang, G., Lei, C., Li, T., & Liu, L. (2013). Low-Temperature Relaxations Associated with Mixed-Valent Structure in Sr_2TiMnO_6. *Journal of the American Ceramic Society*, **96**(2), 513-518.

[17] Kim, K. M., Kim, S. J., Lee, J. H., & Kim, D. Y. (2007). Microstructural evolution and dielectric properties of SiO_2-doped $CaCu_3Ti_4O_{12}$ ceramics. *Journal of the European Ceramic Society*, **27**(13-15), 3991-3995.

[18] Kawrani, S., Boulos, M., Cornu, D., & Bechelany, M. (2019). From synthesis to applications: copper calcium titanate (CCTO) and its magnetic and photocatalytic properties. *ChemistryOpen*, **8**(7), 922.

[19] Kashyap, R., Thakur, O. P., & Tandon, R. P. (2012). Study of structural, dielectric and electrical conduction behaviour of Gd substituted $CaCu_3Ti_4O_{12}$ ceramics. *Ceramics International*, **38**(4), 3029-3037.

[20] Kumari, R., Ahlawat, N., Agarwal, A., Sanghi, S., Sindhu, M., & Rani, S. (2018). Effect of doping of alkaline metal ions on structural and electrical properties of Bi0. 8M0. $2FeO_3$-modified $Na_{0.5}Bi_{0.5}TiO_3$ ceramics (M= Ca, Sr, and Ba). *Journal of Alloys and Compounds*, **747**, 712-720.

[21] Li, M., Chen, X. L., Zhang, D. F., Wang, W. Y., & Wang, W. J. (2010). Humidity sensitive properties of pure and Mg-doped $CaCu_3Ti_4O_{12}$. *Sensors and Actuators B: Chemical*, **147**(2), 447-452.

[22] Lin, Y. H., Deng, W., Xu, W., Liu, Y., Chen, D., Zhang, X., & Nan, C. W. (2012). Abnormal dielectric behaviors in Mn-doped $CaCu_3Ti_4O_{12}$ ceramics and their response mechanism. *Materials Science and Engineering: B*, **177**(20), 1773-1776.

[23] Cai, J., Lin, Y. H., Cheng, B., Nan, C. W., He, J., Wu, Y., & Chen, X. (2007). Dielectric and nonlinear electrical behaviors observed in Mn-doped $CaCu_3Ti_4O_{12}$ ceramic. *Applied Physics Letters*, **91**(25), 252905.

[24] Wang, C., Ni, W., Zhang, D., Sun, X., Wang, J., Li, H., & Zhang, N. (2016). Dielectric properties of pure and Mn-doped $CaCu_3Ti_4O_{12}$ ceramics over a wide temperature range. *Journal of Electroceramics*, **36**(1), 46-57.

[25] Mandal, K. D., Rai, A. K., Kumar, D., & Parkash, O. (2009). Dielectric properties of the $Ca_{1-x}La_xCu_3Ti_{4-x}Co_xO_{12}$ system (x= 0.10, 0.20 and 0.30) synthesized by semi-wet route. *Journal of alloys and compounds*, **478**(1-2), 771-776.

[26] Senda, S., Rhouma, S., Torkani, E., Megriche, A., & Autret, C. (2017). Effect of nickel substitution on electrical and microstructural properties of $CaCu_3Ti_4O_{12}$ ceramic. *Journal of Alloys and Compounds*, **698**, 152-158.

[27] Kim, H. E., Choi, S. M., Hong, Y. W., & Yoo, S. I. (2014). Improved dielectric properties of the $CaCu_3Ti_4O_{12}$ composites using $BaTiO_3$-coated powder as precursor. *Journal of alloys and compounds*, **610**, 594-599.

[28] Gautam, P., Khare, A., Sharma, S., Singh, N. B., & Mandal, K. D. (2016). Characterization of $Bi_{2/3}CaCu_3Ti_4O_{12}$ ceramics synthesized by semi-wet route. *Progress in Natural Science: Materials International*, **26**(6), 567-571.

[29] Jia, R., Zhao, X., Li, J., & Tang, X. (2014). Colossal breakdown electric field and dielectric response of Al-doped $CaCu_3Ti_4O_{12}$ ceramics. *Materials Science and Engineering: B*, **185**, 79-85.

[30] Sun, D. L., Wu, A. Y., & Yin, S. T. (2008). Structure, properties, and impedance spectroscopy of $CaCu_3Ti_4O_{12}$ ceramics prepared by sol–gel process. *Journal of the American Ceramic Society*, **91**(1), 169-173.

[31] Wu, X., Huang, K., Yuan, L., & Feng, S. (2018). Fabrication of ultralong perovskite structure nanotubes. *RSC advances*, **8**(1), 367-373.

[32] Huang, C. J., Li, K., Wu, S. Y., Zhu, X. L., & Chen, X. M. (2015). Variation of ferroelectric hysteresis loop with temperature in $(Sr_xBa_{1-x})Nb_2O_6$ unfilled tungsten bronze ceramics. *Journal of Materiomics*, **1**(2), 146-152.

[33] Yadava, S. S., Singh, L., Sharma, S., Mandal, K. D., & Singh, N. B. (2016). Effect of temperature on the dielectric and ferroelectric properties of a nanocrystalline hexagonal $Ba_4YMn_3O_{11.5-\delta}$ ceramic synthesized by a chemical route. *RSC Advances*, **6**(72), 68247-68253.

CHAPTER – 5

Studies of sintering temperature on the microstructure, magnetic and dielectric behavior of $CaCu_3Ti_{3.5}Mn_{0.5}O_{12}$ ceramic synthesized by semi-wet route

5.1. Introduction

The $CaCu_3Ti_4O_{12}$ (CCTO) has fascinated much importance due to the extraordinary perovskite structure and unexpected dialectical behavior. The calcium copper titanate ceramic has been combined with 1:3 ratio A-site ordered perovskite $A_1Cu_3Ti_4O_{12}$ with space group Im3, combining the octahedral Ti-site of TiO_6 and also jointed with A-site of Cu square-planar [1, 2]. The CCTO ceramic type of perovskite containing giant dielectric constant with high tangent loss (tan δ) and sensitivity of dielectric behaviors depend on the method of preparation [2]. Seriously, the major problem in the application of CCTO is high tangent loss which urgently needs to develop a stable processing method. Till now, some theoretical method has been suggested to describe the origin of high dielectric permittivity and low dielectric loss (tan δ) which finally assist to build up applications of CCTO perovskite material. These methods are internal domain [3], electrode polarization effect [4], bimodal grain size model [5], internal barrier layer capacitance (IBLC) [6], and nanoscale barrier layer capacitance model (NBLC) [7]. The abnormal behavior of CCTO ceramic is most successfully described by the internal barrier layer capacitance (IBLC) model [8, 9]. This model suggests that *n*-type semiconducting grains are separated by insulating barriers corresponding to the Ti-rich secondary phase observed in grains boundaries [10, 25], creating a lot of insignificant capacitances and resulting in giant abnormal dielectric constant values. Afterward, the NBLC model also explained the behavior of dielectric constant on the basis of the existence of stacking faults by reconciling the opposing view of the intrinsic and extrinsic nature of Mn-doped CCTO ceramic [7]. Few of the occasions, dielectric loss, and non-linear permittivity were also explained by the different models and their results suggested that these are strongly associated with the microstructure of CCTO

ceramic type of perovskite complexes which can be influenced by elemental doping and sintering condition [6, 11, 12]. The permittivity of CCTO ceramic was extremely depending on the preparation method, e.g., the dielectric function was also increased from 10^3 to 10^4 by varying the sintering temperature from 1000°C to 1100°C [13]. Interestingly, during sintering, the dielectric constant was increased with the grain's growth and decrease with the resistance of grain boundaries [3,5]. In the last decade, the CCTO perovskite-type of oxides achieved immense attention owing to their significance and potential impact in a ceramic capacitor, microwave device applications and other electronic devices [14].

In present work, we have synthesized the $CaCu_3Ti_{3.5}Mn_{0.5}O_{12}$ ceramic via the semi-wet method and their relative studies of magnetic, dielectric properties and their microstructures of CCTMO sintered (for 8 h) at 950°C, 1050°C, and 1100°C, respectively for 8 h [24]. This procedure possesses the benefit to upgrade dielectric function, tangent loss and magnetic behavior of $CaCu_3Ti_{3.5}Mn_{0.5}O_{12}$ ceramic.

5.2. Experimental

5.2.1. Synthesis

The Mn-doped CCTO was manufactured by the semi-wet method. Firstly in this technique, Mn-doped CCTO was synthesized through semi-wet route by using different analytical grade calcium nitrate, $Ca(NO_3)_2.4H_2O$ (98% Merck, India), Copper nitrate, $Cu(NO_3)_2.3H_2O$ (99% Merck, India), Manganese acetate, $Mn(CH_3COO)_2.4H2O$ (99% Merck, India), and titanium oxide, TiO_2 (99% Merck, India), as a starting material in stoichiometric amount in molar ratio. The stoichiometric amount of $Ca(NO_3)_2.4H_2O$, $Cu(NO_3)_2.3H_2O$ and $Mn(CH_3COO)_2.4H_2O$ were taken in double-distilled water.

All the prepared solutions were mixed simultaneously in a beaker and the solid TiO_2 was taken in the stoichiometric amount in the solution. The stoichiometric amount of citric acid (99.5%, Merck India) equivalent to metal ions was added in solution and mixed with each other. The resultant solution was heated on a hot plate magnetic stirrer at 70°C-80°C to evaporate water and allows for self-ignition. The ignition procedure occurred in the air, which produced a grouping of gases and formed a fluffy mass of Mn-doped CCTO powders. Citric acid acts as a complexing agent that used as fuel which helps in the ignition step. The consequential Mn-doped CCTO was ground by using agate and mortar to form a fine powder. The CCTMO fine powder was calcined at 800°C for 7 h. The calcined powder was used to create for cylindrical pellets with the using of 3% polyvinyl alcohol as a binder on applying 3 tons of pressure using hydraulic pressure for 120 seconds. Finally, the Mn-doped CCTO pellets were sintered at 950°C, 1050°C, and 1100°C, respectively for 8 h.

5.2.2. Characterization

The phase of Mn-doped CCTO perovskite sintered was recognized by an XRD (Rigaku mini flex 600, Japan) applying Cu-kα radiation with wavelength 1.5418 A^0. The morphology, as well as elemental composition, was examined by SEM (ZEISS; model EVO18 research, Germany) attached with an energy-dispersive X-ray analyzer (Oxford instrument, USA). The particle size was confirmed through a TEM (TEM, Technai G2 20 S-Twin). For TEM characterization, the sample was suspended in ethanol and sonicated 2 h. This suspension was dispersed on a carbon-coated copper grid and dried in oven 4 h. The thickness, as well as surface morphology, were analyzed using Atomic force microscopy (NTEGRA Prima, Germany).

The magnetic behavior of Mn-doped CCTO was determined by Quantum Design MPMS-3, over a temperature range of 5 to 300 K at magnetic field ± 2 T. Temperature difference of zero-field cooled was determined at 100 Oe applied field were carried out using SQUID VSM dc magnetometer. The dielectric information of silver-coated cylindrical pellets was determined by LCR meter (PSM1735, NumetriQN$_4$L, and U.K.).

5.3. Results and Discussion

5.3.1. X-ray diffraction studies

The phase of $CaCu_3Ti_{3.5}Mn_{0.5}O_{12}$ (CCTMO) ceramic powder confirmed by XRD sintered at 950^{o}C, 1050^{o}C, and 1100^{o}C, respectively for 8 h, depicts in Fig. 5.1. It shows the existence of CCTO as the main phase along with the slightly secondary phase of TiO_2. The diffraction patterns are exactly matched with JCPDS (card no.21-0140), which confirms the occurrence of the main phase formation of CCTO with the slight secondary phase with JCPDS (card no.46-1238) of TiO_2 [15].

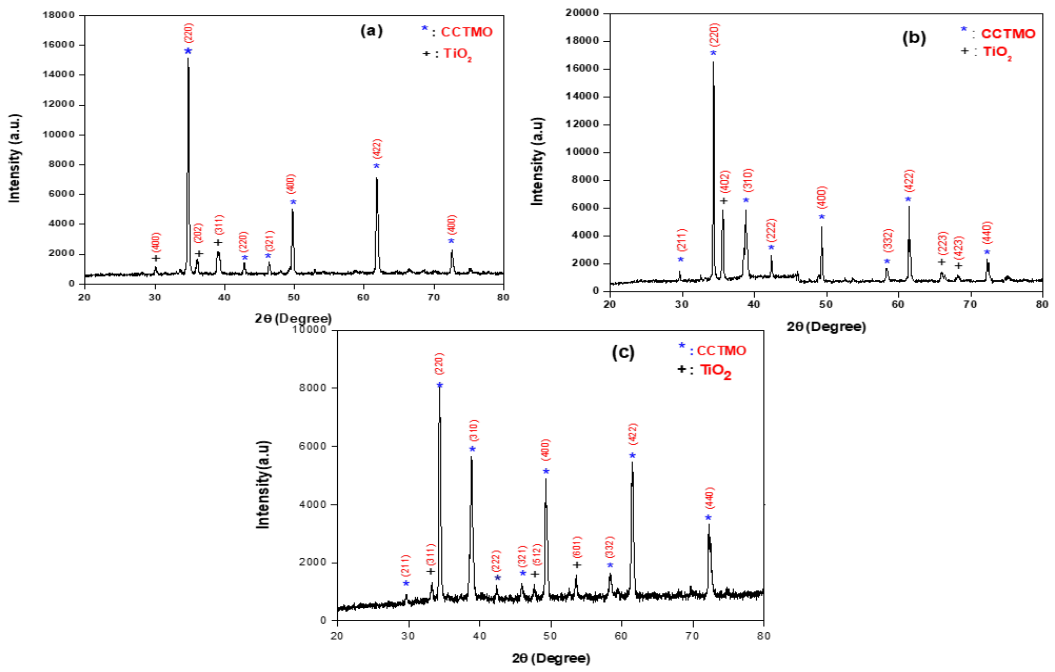

Fig. 5.1. XRD patterns of CCTMO sintered at (a) 1223 K (b) 1323 K (c) 1373 K for 8 h.

The crystalline size (D) of $CaCu_3Ti_{3.5}Mn_{0.5}O_{12}$ was determined through the Debye Scherrer equation, which is shown below in eq. (1).

$$D = \frac{K\lambda}{\beta COS\theta} \quad (1)$$

where D is crystallite size, k is constant equal to 0.89, λ is a wavelength of X-ray, θ is the Bragg diffraction angle and β is the full width at half maximum (FWHM) in radians. For the determination of the accurate value of crystalline size, the line broadening due to instrumental effect removed by adding a standard sample for XRD data. The average crystallite size of $CaCu_3Ti_{3.5}Mn_{0.5}O_{12}$ was calculated 38.97 ± 10 nm, 69.32 ± 10 nm and 36.54 ± 10 nm at 950 ^oC, 1050 ^oC, and 1100 ^oC, for 8 h, respectively.

5.3.2. Microstructural studies

Figure 5.2a-c presents the bright-field TEM images of $CaCu_3Ti_{3.5}Mn_{0.5}O_{12}$ (CCTMO) sintered at 950 ^oC, 1050 ^oC, and 1100 ^oC, respectively for 8 h. The particle size of CCTMO calculated by TEM is found to be 98.49 ± 10 nm, 92.95 ± 10 nm and 145.50 ± 10 nm at 950 ^oC, 1050 ^oC, and 1100 ^oC, respectively. The particle size is found to be dependent upon sintering temperature as the sintering temperature increases particle size also increases. The particle size and average crystallite size are closed with each other determined by TEM as well as XRD. The selected area diffraction pattern (SEAD) is also shown in Fig. 5.2(d) of $CaCu_3Ti_{3.5}Mn_{0.5}O_{12}$ ceramic sintered at 1100^{o}C which is confirmed the existence of single-phase nanocrystalline materials.

The diffraction pattern was indexed according to a cubic crystal structure and the calculated lattice parameter was found to be 7.393 Å. The lattice parameter observed from the SEAD pattern was in good agreement with the value obtained from the JCPDS card no. 21-0140 for XRD data.

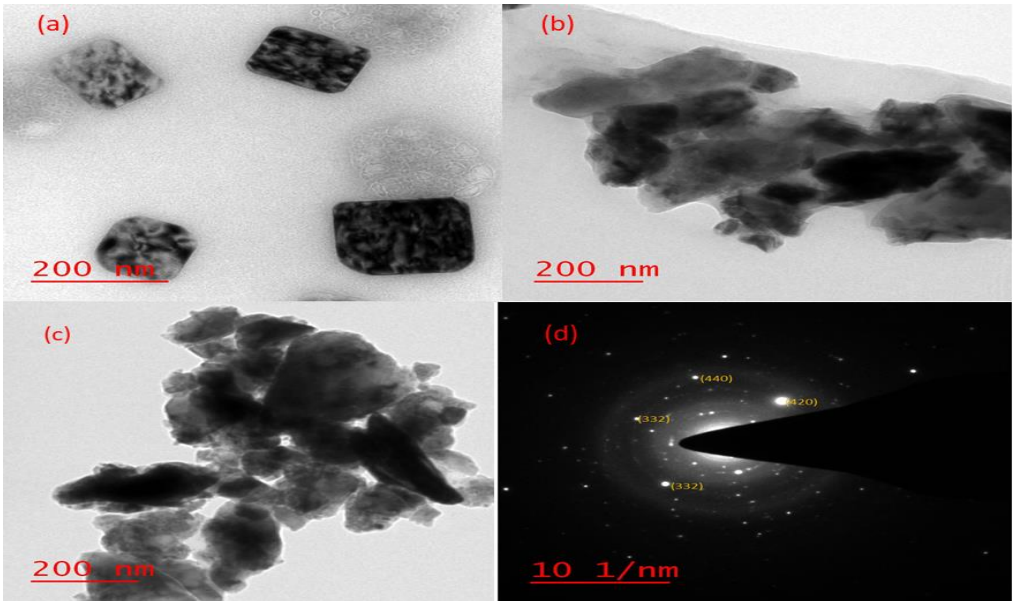

Fig. 5.2. Bright-field TEM images at (a) 1223 K (b) 1323 K (c) 1373 K and (d) Selected area diffraction pattern of CCTMO at 1373 K.

Figure 5.3 (a-c) shows the SEM micrograph of $CaCu_3Ti_{3.5}Mn_{0.5}O_{12}$ ceramic sample sintered at 950ºC, 1050ºC, and 1100ºC, respectively for 8 h. The substituting of Mn in $CaCu_3Ti_4O_{12}$ significantly affects the surface morphology [16]. The grain size of $CaCu_3Ti_{3.5}Mn_{0.5}O_{12}$ ceramic at low temperature i.e. 950ºC shows large-grained with grain size 1.05 ± 10 µm. The grain size of $CaCu_3Ti_{3.5}Mn_{0.5}O_{12}$ ceramic at high temperature i.e. 1050ºC as well as 1100ºC is about 9.50 ± 10 µm and 14.87 ± 10 µm, respectively. The grain size regularly increases with respect to temperature. In general, at low-temperature grain boundaries are not clear but at high-temperature grains and

grain boundary, both are clearly visible in Fig. 5.3(b-c). The increase the grain size with respect to the temperature of CCTMO ceramic may be due to enlarged grain boundary mobility. The Fig. 5.3(d-f) shows the EDX spectra of Mn-doped CCTO ceramic sintered at 950^{o}C, 1050^{o}C, and 1100^{o}C, respectively for 8h [25] respectively for 8h, which verify the existence of Ca, Cu, Mn, Ti, and O elements. The atomic percentage of Ca, Cu, Mn, Ti, and O elements are present in table 5.1 with different temperatures were confirmed the stoichiometry and purity of the materials.

Table 5.1. Atomic percentage of elements for $CaCu_3Ti_{3.5}Mn_{0.5}O_{12}$ sintered at 1223 K, 1323 K and 1373 K, respectively for 8 h.

Temperature	atomic percent of elements				
	Ca	Cu	Ti	Mn	O
1223 K	5.09 %	14.44 %	18.60 %	2.32 %	59.55 %
1323 K	3.47 %	39.71 %	8.87 %	1.97 %	46.09 %
1373 K	3.39 %	32.78 %	8.71 %	1.68 %	53.44 %

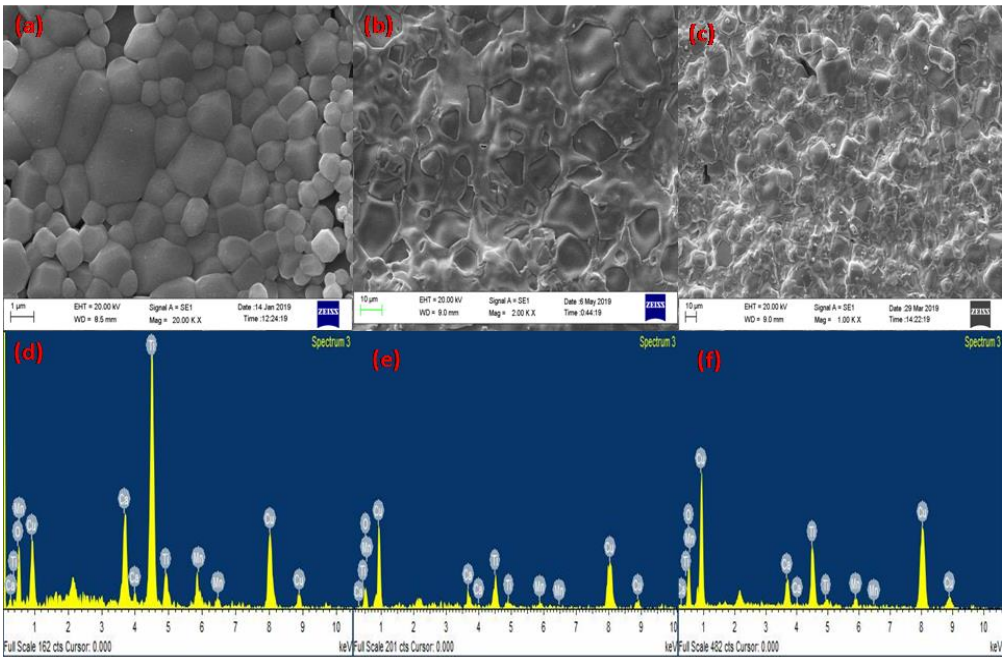

Fig. 5.3. (a-c) SEM micrograph and (d-e) EDX spectra of CCTMO ceramic sintered at 1223 K, 1323 K, and 1373 K, respectively for 8 h.

Figure 5.4(a) present 2-D Atomic Force Micrograph (AFM) of $CaCu_3Ti_{3.5}Mn_{0.5}O_{12}$ ceramic sintered at 1100^{o}C for 8h, which shows cubical structures of grain unconnected by a grain boundary. The average roughness (R_a), as well as root, mean square roughness (R_q) was obtained as 7.55 nm and 9.23 nm, respectively on a scanned area 5.0 µm × 5.0 µm. Fig. 5.4(b) depict the distribution of particle on the surface which was observed in the 3-D structure. The grain size determined by the histogram graph occurs in the range of 0.8 µm-1.5 µm and the average particle size was found to be 0.44 µm out of the 514 grains shown in Fig. 5.4(c).

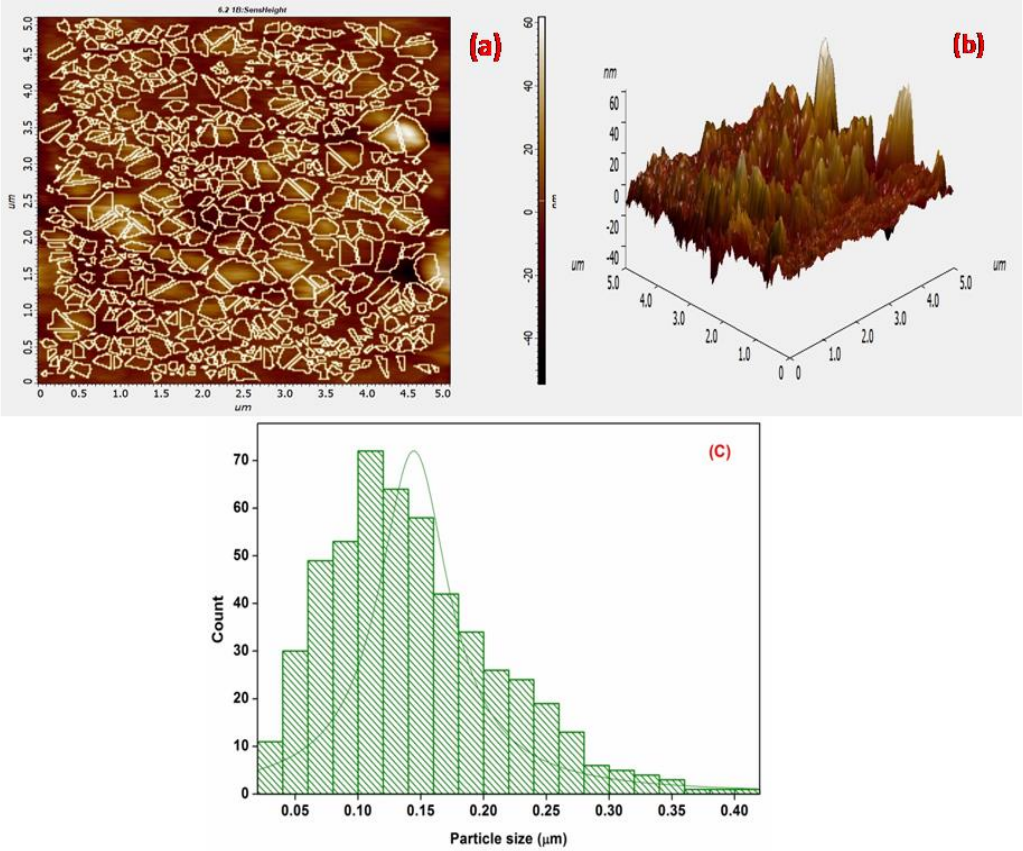

Fig. 5.4. AFM images of CCTMO ceramics sintered at 1373 K for 8 hours (a) 2-dimensional structure (b) 3-dimensional structure (c) bar diagram of particle size.

5.3.3. Magnetic studies

In order to prove the magnetization behavior of Mn-doped CCTO ceramic sintered 1100^{o}C for h, the temperature dependence of ZFC and FC magnetization was recorded in a temperature range of 5-300 K with 100 Oe as an applied field shown in Fig. 5.5(a).The transitions show between ZFC and FC just about at 114 K. The magnetization increases quickly in the FC curve that proves the existence of ferromagnetic behavior of CCTMO ceramic. Meanwhile, in CCTMO ceramic only one critical temperature is detecting around 114 K [17]. However, CCTMO ceramic ZFC and FC curve decrease with increasing temperature.

The M-H hysteresis curves measured at two different temperatures (5, 300 K) and applied field ± 2 T for $CaCu_3Ti_{3.5}Mn_{0.5}O_{12}$ is depicted in Fig. 5.5(b). The M-H hysteresis curves display a linear behavior similar to the anti-ferromagnetic system at 5 K. Further, the linear behavior in the magnetic moment along with the magnetic field is recorded with an increase of temperature (300 K) which confirms the existence of paramagnetic behavior of the material [18].

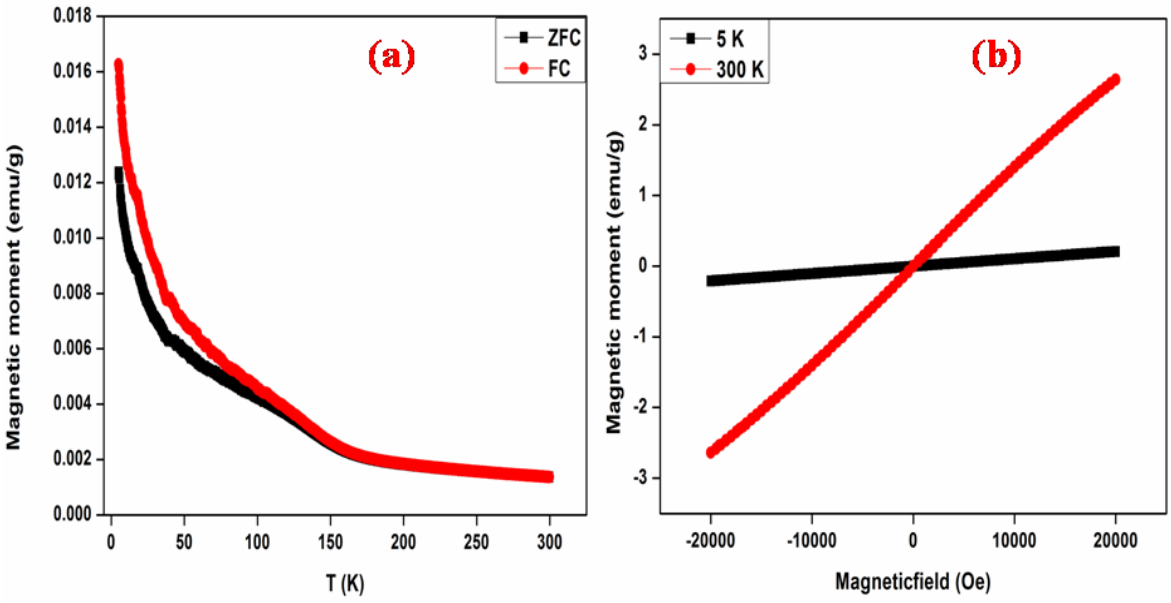

Fig. 5.5. Temperature-dependent (a) magnetic moment noted applied magnetic field at 100 Oe. (b) M-H hysteresis at 5 and 300 K for CCTMO ceramic sintered at 1323 K for 8 h.

Fig. 5.6 describes the temperature-dependent reciprocal of magnetic susceptibility for $CaCu_3Ti_{3.5}Mn_{0.5}O_{12}$ ceramic. The Weiss temperature (θ) and Curie constant (C) can be determined by using the Curie–Weiss law, represented by the following equation.

$$\chi = \frac{C}{T-\theta} \qquad (2)$$

Where, χ is magnetic susceptibility, C is curie constant, θ is Curie Weiss temperature and T is temperature. The calculated value of Curie constant (C) and Weiss temperature (θ) obtained by this plot was found to be 5811.76 emus/g^{-1} and 57.04 K, respectively. The positive value of θ confirms the ferromagnetic behavior of Mn-doped CCTO ceramic.

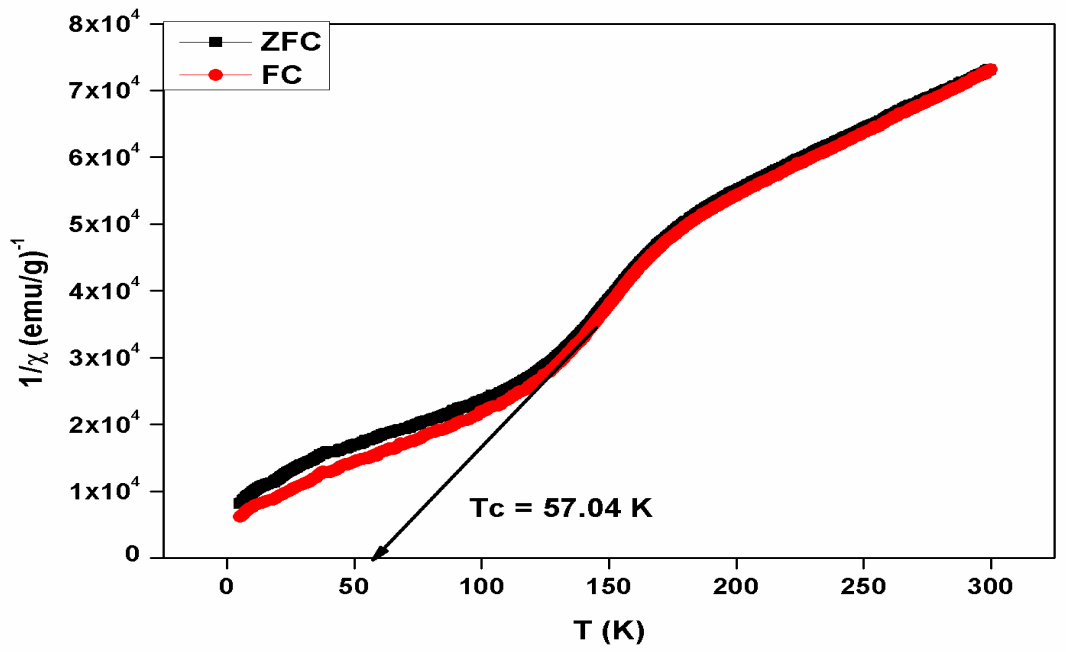

Fig. 5.6. Magnetic susceptibility as a function of temperature recorded at ± 2 T and applied magnetic field (H) at 100 Oe.

Figure 5.7 depicts the polarization against the electric field P-E hysteresis loop of $CaCu_3Ti_{3.5}Mn_{0.5}O_{12}$ ceramic was detected at room temperature (35^oC). This estimation was carried out at a frequency of 150 Hz. As the increasing temperature, the nature of the loop has been changed to become slimmer. This type of behavior of the P-E loop represents the evolution process of relaxor ferroelectrics [19].

By applying the electric field resultant remnant polarization (Pr) increases with increasing sintering temperature of $CaCu_3Ti_{3.5}Mn_{0.5}O_{12}$ materials. The measured remnant polarization (Pr) of CCTMO ceramic is 0.827, 0.989 and 1.005 μC/cm^2 at 1223 K, 1323 K and 1373 K, respectively. On the applying, high electric field saturation has not occurred in the P-E loop which might be due to the combined effect of capacitor and resistor joint in parallel (lossy capacitor) of these materials [20].

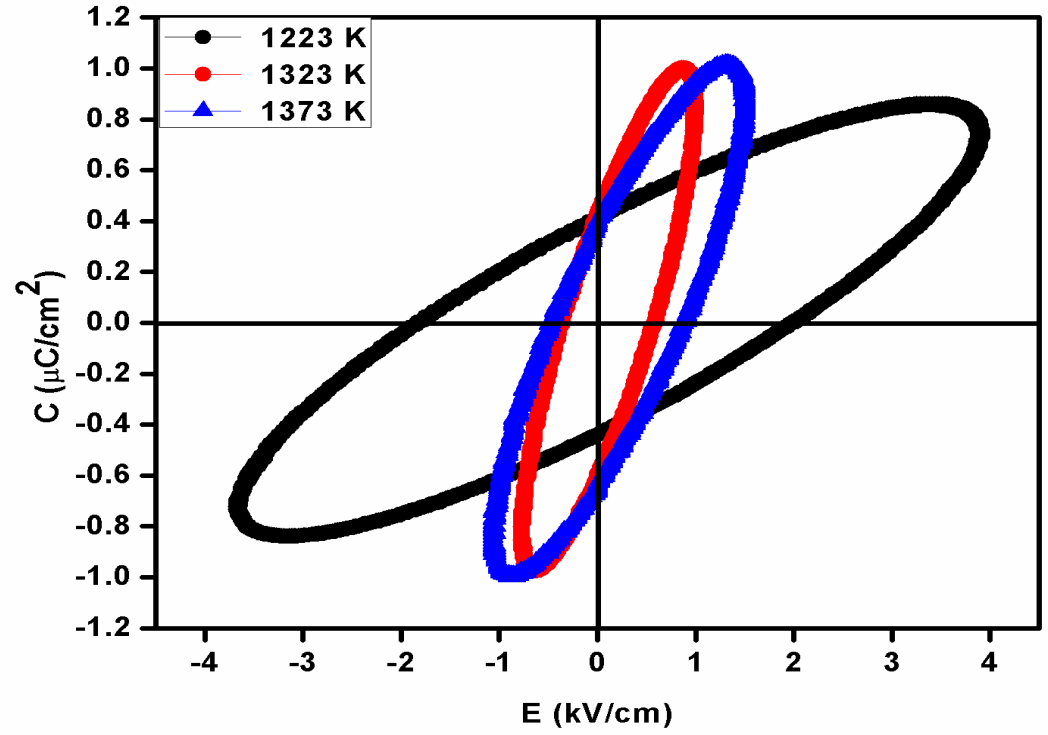

Fig. 5.7. The polarization versus electric field (P-E) hysteresis loop of $CaCu_3Ti_{3.5}Mn_{0.5}O_{12}$ at sintered at 1223 K, 1323 K, and 1373 K, respectively.

5.3.4. Dielectric studies

Figure 5.8 depicts the results of temperature-dependent dielectric function (ε_r) and tangent loss (tan δ) at 10 kHz for sintered 950°C, 1050°C, and 1100°C, respectively for 8 h.

The data specify that the $CaCu_3Ti_{3.5}Mn_{0.5}O_{12}$ ceramic depicts an important effect on the dielectric behavior at 35°C (r t). The variation in dielectric function (ε_r) can be assigned to the differences in the grain size distribution. Mn-doped CCTO ceramic has a lower permittivity (ε_r) than pure CCTO ceramic sample [21]. The dielectric function of pure CCTO indicates the giant value around 20,000 at 300 K, but the value of dielectric function decreases abruptly with a decreasing temperature below 120 K [22]. The dielectric function increases with increasing temperature due to the capability of the charge carriers to an alien with applied field increases at higher temperatures [21]. However, we observed that the value of the dielectric function of CCTMO decreases from 25,000 to 100 at 300 K (R.T) shows in Fig. 5.8 (a). This result is clearly confirmed that little quantity of Mn-doping on the Ti-sites in CCTO produced an astonishing effect on dielectric behaviors of CCTMO ceramic. In Fig. 5.8 (a) we found that the value of dielectric function increases with rising sintering temperature [23]. The values of dielectric function are found to be 40, 90 and 95 at 10 kHz for sintering temperature at 950°C, 1050°C, and 1100°C, respectively for 8 h. The tangent loss (tan δ) increases slightly from 300 K to 380 K, and thereafter rises quickly with rising temperature to 508 K for all sintering temperatures shows in Fig. 5.8 (b). The value of tangent loss (tan δ) was obtained to be less than 0.3 at 10 kHz for all sintering temperatures.

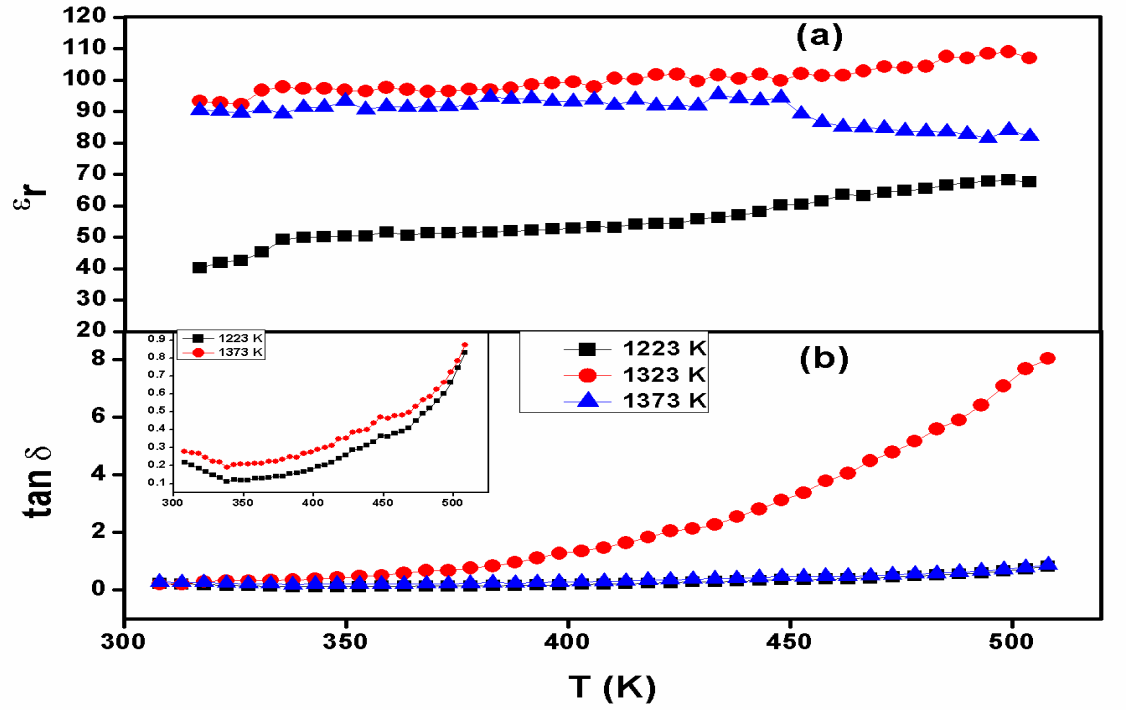

Fig. 5.8. Temperature-dependent (a) dielectric constant (Ɛr) and (b) loss tangent (tan δ) at 10 kHz for sintered at 1223 K, 1323 K, and 1373 K, respectively for 8 h.

Figure 5.9 presents the frequency-dependent dielectric function (ε_r) and tangent loss (tan δ) at room temperature for sintered at 950 ^oC, 1050 ^oC, and 1100 ^oC, respectively for 8 h. The value of the dielectric function (ε_r) is found to be 200, 260 and 00 at sintering temperature 950 ^oC, 1050 ^oC, and 1100 ^oC respectively shows in Fig. 5.9 (a). However, the Mn-doping decreases dielectric constant (ε_r) and in fact refine the tangent loss (tan δ) at room temperature at around medium frequency region. The tangent loss (tan δ) is found to be less than 0.5 for all sintering temperature shows in Fig. 5.9 (b).

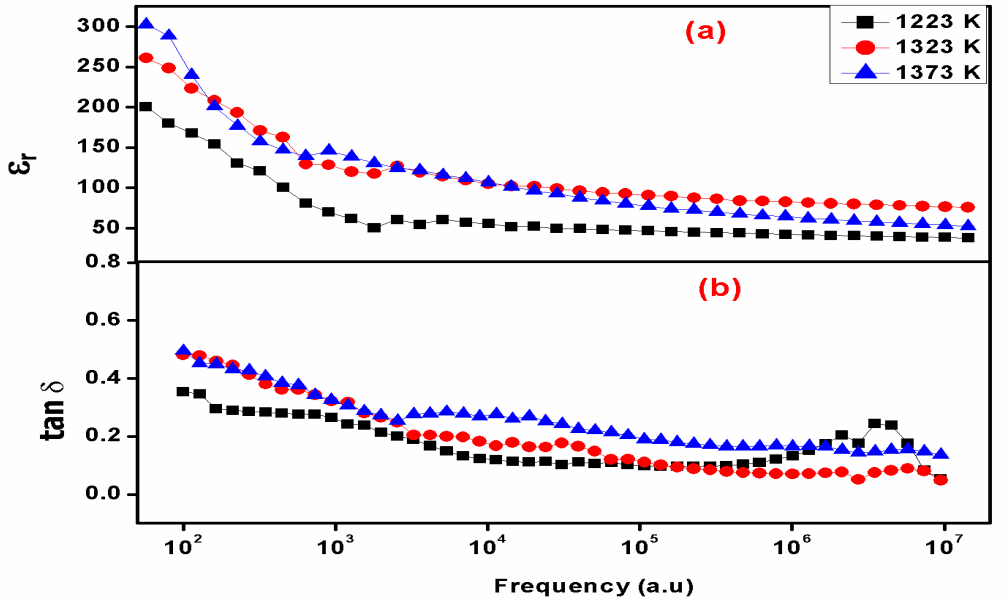

Fig. 5.9. Frequency-dependent (a) dielectric constant (Ɛr) and (b) loss tangent (tan δ) at room temperature for sintered at 1223 K, 1323 K, and 1373 K, respectively.

5.4. Conclusions

The Mn-doped calcium copper titanium oxide; $CaCu_3Ti_4O_{12}$ was prepared by the semi-wet route. The phase of CCTMO was detected by XRD and crystallite size obtained from the XRD data were occurred to be 38.97 ± 10 nm, 69.32 ± 10 nm and 36.54 ± 10 nm at 950°C, 1050°C, and 1100°C, for 8 h, respectively. The particle size obtained by TEM is 98.49 ± 10 nm, 92.95 ± 10 nm and 145.50 ± 10 nm at 950°C, 1050°C, and 1100°C, respectively. The EDX spectra confirmed that the presence of Ca, Cu, Ti, Mn, O element in $CaCu_3Ti_{3.5}Mn_{0.5}O_{12}$ ceramic in stoichiometric ratio as the molecular formula. The dielectric function (ε_r) and tangent loss were occurred to be 40-300 and 0.2-0.6 at room temperature. The dielectric function increases and tangent loss decreases with increasing sintering temperature.

[1] Subramanian, M. A., & Sleight, A. W. (2002). $ACu_3Ti_4O_{12}$ and $ACu_3Ru_4O_{12}$ perovskites: high dielectric constants and valence degeneracy. *Solid state sciences*, **4**(3), 347-351.

[2] Schmidt, R., Stennett, M. C., Hyatt, N. C., Pokorny, J., Prado-Gonjal, J., Li, M., & Sinclair, D. C. (2012). Effects of sintering temperature on the internal barrier layer capacitor (IBLC) structure in Ca $Cu_3Ti_4O_{12}$ (CCTO) ceramics. *Journal of the European Ceramic Society*, **32**(12), 3313-3323.

[3] Fang, T. T., & Liu, C. P. (2005). Evidence of the internal domains for inducing the anomalously high dielectric constant of Ca $Cu_3Ti_4O_{12}$. *Chemistry of Materials*, **17**(20), 5167-5171.

[4] Lunkenheimer, P., Fichtl, R., Ebbinghaus, S. G., & Loidl, A. (2004). Nonintrinsic origin of the colossal dielectric constants in $CaCu_3Ti_4O_{12}$. *Physical review B*, **70**(17), 172102.

[5] Pan, M. J., & Bender, B. A. (2005). A bimodal grain size model for predicting the dielectric constant of calcium copper titanate ceramics. *Journal of the American Ceramic Society*, **88**(9), 2611-2614.

[6] Senda, S., Rhouma, S., Torkani, E., Megriche, A., & Autret, C. (2017). Effect of nickel substitution on electrical and microstructural properties of $CaCu_3Ti_4O_{12}$ ceramic. *Journal of Alloys and Compounds*, **698**, 152-158.

[7] Bueno, P. R., Tararan, R., Parra, R., Joanni, E., Ramirez, M. A., Ribeiro, W. C., ... & Varela, J. A. (2009). A polaronic stacking fault defect model for $CaCu_3Ti_4O_{12}$ material: an approach for the origin of the huge dielectric constant and semiconducting coexistent features. *Journal of Physics D: Applied Physics*, **42**(5), 055404.

[8] Fiorenza, P., Lo Nigro, R., Bongiorno, C., Raineri, V., Ferarrelli, M. C., Sinclair, D. C., & West, A. R. (2008). Localized electrical characterization of the giant permittivity effect in $CaCu_3Ti_4O_{12}$ ceramics. *Applied Physics Letters*, **92**(18), 182907.

[9] Singh, L., Rai, U. S., & Mandal, K. D. (2013). Dielectric, modulus and impedance spectroscopic studies of nanostructured $CaCu_{2.70}Mg_{0.30}Ti_4O_{12}$ electro-ceramic synthesized by modified sol–gel route. *Journal of alloys and compounds*, **555**, 176-183.

[10] Fernandez, J. F., Leret, P., Romero, J. J., De Frutos, J., De La Rubia, M. Á., Martín-González, M. S., & García, M. Á. (2009). Proofs of the coexistence of two magnetic contributions in pure and doped $CaCu_3Ti_4O_{12}$ giant dielectric constant ceramics. *Journal of the American Ceramic Society*, **92**(10), 2311-2318.

[11] Li, T., Chen, J., Liu, D., Zhang, Z., Chen, Z., Li, Z., ... & Wang, B. (2014). Effect of NiO-doping on the microstructure and the dielectric properties of $CaCu_3Ti_4O_{12}$ ceramics. *Ceramics International*, **40**(7), 9061-9067.

[12] Zheng, Q., Fan, H., & Long, C. (2012). Microstructures and electrical responses of pure and chromium-doped $CaCu_3Ti_4O_{12}$ ceramics. *Journal of alloys and compounds*, **511**(1), 90-94.

[13] Bender, B. A., & Pan, M. J. (2005). The effect of processing on the giant dielectric properties of $CaCu_3Ti_4O_{12}$. *Materials Science and Engineering: B*, **117**(3), 339-347.

[14] Shay, D. P., Podraza, N. J., Donnelly, N. J., & Randall, C. A. (2012). High energy density, high temperature capacitors utilizing Mn-doped $0.8CaTiO_3–0.2CaHfO_3$ ceramics. *Journal of the American Ceramic Society*, **95**(4), 1348-1355.

[15] Cai, J., Lin, Y. H., Cheng, B., Nan, C. W., He, J., Wu, Y., & Chen, X. (2007). Dielectric and nonlinear electrical behaviors observed in Mn-doped $CaCu_3Ti_4O_{12}$ ceramic. *Applied Physics Letters*, **91**(25), 252905.

[16] Xu, Z., & Qiang, H. (2017). Enhanced dielectric properties of Zn and Mn co-doped $CaCu_3Ti_4O_{12}$ ceramics. *Journal of Materials Science: Materials in Electronics*, **28**(1), 376-380.

[17] Han, D., Wu, Z., Wang, Z., & Yang, S. (2016). Oriented Mn-doped CuO nanowire arrays. *Nanotechnology*, **27**(13), 135603.

[18] Pal, K., Dey, A., Ray, P. P., Mordvinova, N. E., Lebedev, O. I., Mandal, T. K., ... & Gayen, A. (2018). Synthesis, Characterization and Catalytic Activity of Quadruple Perovskite: $CaCu_{3-x}Mn_xTi_{4-x}Mn_xO_{12}$ (x= 0, 0.5 and 1.0). *Chemistry Select*, **3**(4), 1076-1087.

[19] Huang, C. J., Li, K., Wu, S. Y., Zhu, X. L., & Chen, X. M. (2015). Variation of ferroelectric hysteresis loop with temperature in $(Sr_xBa_{1-x})Nb_2O_6$ unfilled tungsten bronze ceramics. *Journal of Materiomics*, **1**(2), 146-152.

[20] Stewart, M. G. C. M., Cain, M. G., & Hall, D. A. (1999). *Ferroelectric hysteresis measurement and analysis*. Teddington: National Physical Laboratory.

[21] Xu, Z., & Qiang, H. (2017). Enhanced dielectric properties of Zn and Mn co-doped $CaCu_3Ti_4O_{12}$ ceramics. *Journal of Materials Science: Materials in Electronics*, **28**(1), 376-380.

[22] Chung, S. Y., Kim, I. D., & Kang, S. J. L. (2004). Strong nonlinear current–voltage behaviour in perovskite-derivative calcium copper titanate. *Nature materials*, **3**(11), 774-778.

[23] Krohns, S., Lunkenheimer, P., Ebbinghaus, S. G., & Loidl, A. (2008). Colossal dielectric constants in single-crystalline and ceramic $CaCu_3Ti_4O_{12}$ investigated by broadband dielectric spectroscopy. *Journal of Applied Physics*, **103**(8), 084107.

[24] Pandey, S., Kumar, A., Singh, N. B., & Mandal, K. D. (2020). Studies on dielectric and magnetic properties of $CaCu_3Ti_4O_{12}$ ceramic synthesized via semi-wet route. *Journal of the Australian Ceramic Society*, **56**(3), 915-922.

[25] Pandey, S., & Mandal, K. D. (2019). Investigation of microstructure, ferroelectric and dielectric behavior of $CaCu_3Ti_{(4-x)}Mn_xO_{12}$ perovskites synthesized through semi-wet route. *SN Applied Sciences*, **1**(12), 1-7.

[26] Jaiswar, S., & Mandal, K. D. (2017). Evidence of enhanced oxygen vacancy defects inducing ferromagnetism in multiferroic $CaMn_7O_{12}$ manganite with sintering time. *The Journal of Physical Chemistry C*, **121**(36), 19586-19601.

CHAPTER – 6

Effect of doping metal ions on microstructural evolution and dielectric behaviors of $CaCu_3Ti_4O_{12}$ ceramics synthesized by semi-wet route

6.1 Introduction

Due to their significance and potential impact in a ceramic condenser, microwave device applications, and other electronic devices [1, 2], the ABO_3 (A and B cations of dissimilar sizes (B is less than A) and O is the anion) type of ceramic peroxides have attracted more in recent decades. Compared to traditional ferroelectric materials, the $CaCu_3Ti_4O_{12}$ (CCTO), which belongs to the ABO_3 family with a large dielectric constant, is the best choice (around 10^4-10^6). The calcium copper titanate (CCTO) has a cubic structure containing space group Im3 and the parameter for the lattices is 7.391 A^o [2, 3]. The dielectric behavior of CCTO peroxide has been refined by the different cationic substitutions as well as doping at Cu and Ti sites [4, 5]. By controlling the chemistry and microstructure of grain boundaries, cationic substitutions in CCTO directly affect the dielectric function, tangent loss, and electrical behavior. There are two forms of doping or replacement: both acceptor and donor. The accepter cationic substitutions are described as cations (Cu-site) with ionic charges lower than the ions they replace. The donor cationic substitutions are explained as cations with a higher ionic charge than the ions they replace, causing vacancies in the donor substituent CCTO perovskite structures [5, 7]. In complex perovskite structure, the acceptor doping metal ions are generally applied at B-site or Ti-site. Mn^{2+}, Mn^{3+}, Co^{2+}, Co^{3+}, Fe^{2+}, Fe^{3+}, Ni^{2+} and Zn^{2+} are some example of acceptor dopant. Acceptor dopants like Mn^{3+} on the Ti^{4+} site provide oxygen vacancy but without the liberation of an electron. In some literatures were found element containing 5+ or 6+ like as Nb^{5+}, Ta^{5+} and Sb^{5+} W^{6+} at B-sites (Ti-site) and some elements charge of 3+ like as La^{3+}, Bi^{3+} and Nd^{3+} are usually used in A-site (Ca-site) in CCTO perovskite [8].

The dielectric behavior of CCTO is also directly depending on the processing situation such as synthesized routes [3, 9] sintering temperatures[10] and sintering durations[11], a Synthesis route of $CaCu_3Ti_4O_{12}$ has played an important role in confirming the microstructural, and dielectrical behaviors. In the case of Mn and Fe substituted CCTO [12], these two dopants (metal ions) can cause exceptionally major changes in dielectrical behavior grains and grains boundaries. On the other hand, a remarkable decrease in dielectric constant in these two ceramic systems is still recognized for changes in grain boundaries electrical properties [13]. In recent times, numerous papers describing Y, Zr, and Ta substituted CCTO ceramics have been published. But the results of in these papers are completely different [14, 15]. The CCTO ceramics were synthesized by the use of metal nitrate at high temperatures using a solid-state method. Long reaction time, high calcination, and sintering temperature have been required for this process. Alternatively, during synthesis [16-18] some extra minor secondary phases (CuO, TiO_2, and Cu_2TiO_3) may also come out. On the other hand, the CCTO has also been prepared by a chemical process such as sol-gel using metal alkoxide which gives intimate and uniform metal ion mixing in the stoichiometric ratio. Titanium isopropoxide $Ti(OR)_4$ is very expensive in this route. So, we have synthesized Mn, Nb, and W doped CCTO through a semi-wet route sintered at 950^{o}C, 1050^{o}C, and 1100^{o}C, for 8 h, respectively and their comparative studies of morphology and dielectric behaviors. This procedure has the advantage of improving dielectric constant, dielectric loss, and microstructures of Mn, Nb, and W doped CCTO ceramic.

6.2. Experimental

6.2.1 Materials synthesis

The semi-wet method was used to synthesize the $CaCu_3Ti_{3.5}X_{0.5}O_{12}$ (X= Mn, W, and Nb). Chemicals calcium nitrate, $Ca(NO_3)_2.4H_2O$ (98% Merck, India), copper nitrate, $Cu(NO_3)_2.3H_2O$ (99% Merck, India), manganese acetate, $Mn(CH_3COO)_2.4H_2O$ (99% Merck, India), WO_2 (99% Merck, India), Nb_2O_5 (99% Merck, India) and titanium oxide, TiO_2 (99% Merck, India), were taken stoichiometrically in the molar ratio. Using distilled water was prepared a solution of $Ca(NO_3)_2.4H_2O$, $Cu(NO_3)_2.3H_2O$, and $Mn(CH_3COO)_2.4H_2O$. In a beaker, all solutions were mixed and solid TiO_2 was added in solution. In distilled water, the calculated amount of citric acid (99.5 %, Merck India) equivalent to metal ions was dissolved and mixed with the solution. The resulting solution has been heated to evaporate water on a 60-70^oC hot-plate magnetic stirrer and allows for self-ignition. After the removal of a lot of gases, a residual mass of CCTXO (X= Mn, Nb, and W) powders was obtained. Citric acid used in the ignition step as a complex agent that acts as a fuel. The resultant CCTXO powder was ground to obtain a fine powder by using agate and mortar. The powder was calcined at 850^oC for 6 h. All different calcined powder was used to make for cylindrical pellets with the use of 4 % Pollyvinylalcohol as a binder on applying 5 tons of pressure using hydraulic pressure for 120 seconds. At last, the CCTMO, CCTWO and CCTNO pellets were sintered at 950^oC, 1050^oC, and 1100^oC, for 8 h.

6.2.2 Characterization

An X-ray diffractometer (Rigaku miniflex 600, Japan) applying Cu-kα radiation with wavelength 1.5418 A^{o} was confirmed for the phase of $CaCu_3Ti_{3.5}X_{0.5}O_{12}$ (CCTXO) (X=Mn, W and Nb) ceramic sintered samples. Scanning electron microscope (ZEISS; model EVO18 research, Germany) attached with an energy-dispersive X-ray (EDX) (Oxford instrument, USA) analyzer confirmed the microstructure, as well as the elemental composition. A transmission electron microscope (TEM, Technai G2 20 S-Twin), analyzed the particle size. The samples were distributed in ethanol for TEM analysis, and 2 h sonicated. This suspension was deposited on a carbon-coated copper grid and dried in oven 8 h. LCR meter (PSM1735, NumetriQN4L, U.K.) has tested the dielectric details of silver-coated cylindrical pellets. The XPS investigation was conducted by using Thermo Fisher Scientific Kα (Waltham, MA) in broad scan survey mode and high energy resolution with AlK_{α} (1486.6 eV).

6.3. Results and discussions

6.3.1 X-ray diffraction studies

Fig. 6.1 presents the X-ray diffraction pattern of sintered $CaCu_3Ti_{3.5}X_{0.5}O_{12}$ (X= Mn, W, and Nb) (CCTXO) with a different dopant. It confirms the presence of CCTO as a major phase along with the lesser phase of TiO_2. XRD peak is exactly matched to JCPDS (card no.21-0140), reported the CCTO as the main phase along with TiO_2 minor secondary phase with JCPDS (card no.46-1238) [2, 18, 19, 31]. The crystalline size (D) of CCTXO (X=Mn, W, and Nb) was evaluated by using the Debye Scherrer formula.

$$D = K\lambda/\beta COS\theta \qquad (1)$$

where D is crystalline size, k is constant equal to 0.89, λ is a wavelength of X-ray, θ is the Bragg diffraction angle and β is the full width at half maximum (FWHM) in radians. The line broadening due to instrument effect eliminated by using a standard sample for XRD data to calculate the correct value of the crystalline sizes. The average crystallite size of CCTMO, CCTWO, and CCTNO was calculated 38.97 ± 10 nm, 56.23 ± 10 nm, and 42.41 ± 10 nm, respectively.

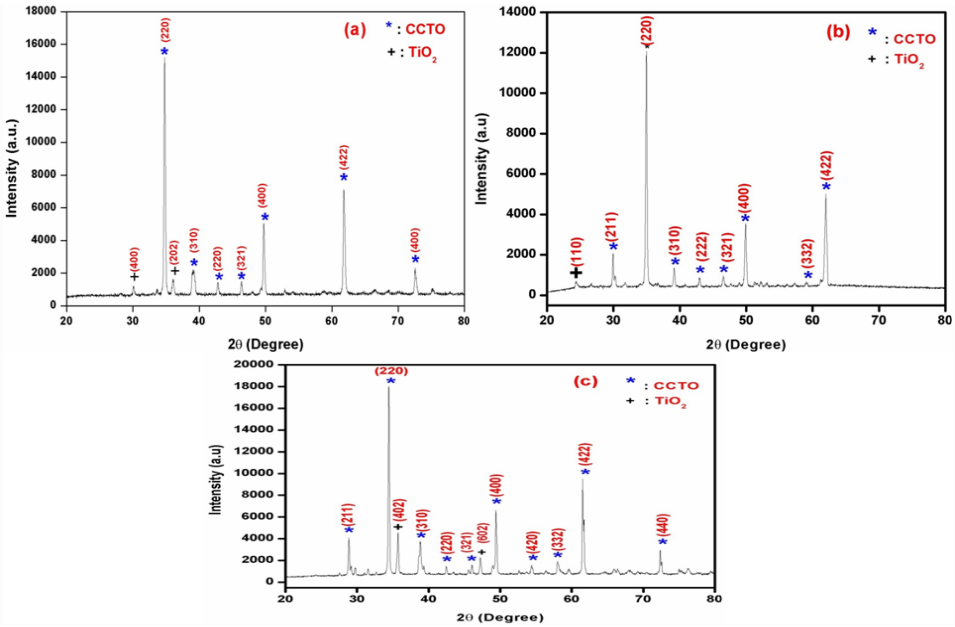

Fig. 6.1. XRD patterns of $CaCu_3Ti_{3.5}X_{0.5}O_{12}$ (a) X= Mn (b) X= Nb (c) X= W sintered at at 1223 K, 1323 K and 1373 K, respectively for 8 h.

6.3.2. Microstructural studies

Fig. 6.2 displays the bright-field TEM images (a, c and e) and their respective selected area diffraction pattern (SEAD) (b, d, and f) of sintered $CaCu_3Ti_{3.5}X_{0.5}O_{12}$ (X= Mn, Nb, and W) (CCTXO) with the different dopant. The observed particles size of CCTMO, CCTNO as well as CCTWO calculated by TEM was found to be 44 nm, 101 nm, and 51

nm, respectively. Figures 6.2(b, d, and f) show the SEAD pattern with single-crystalline in nature which confirms by the free-standing crystal [18, 20].

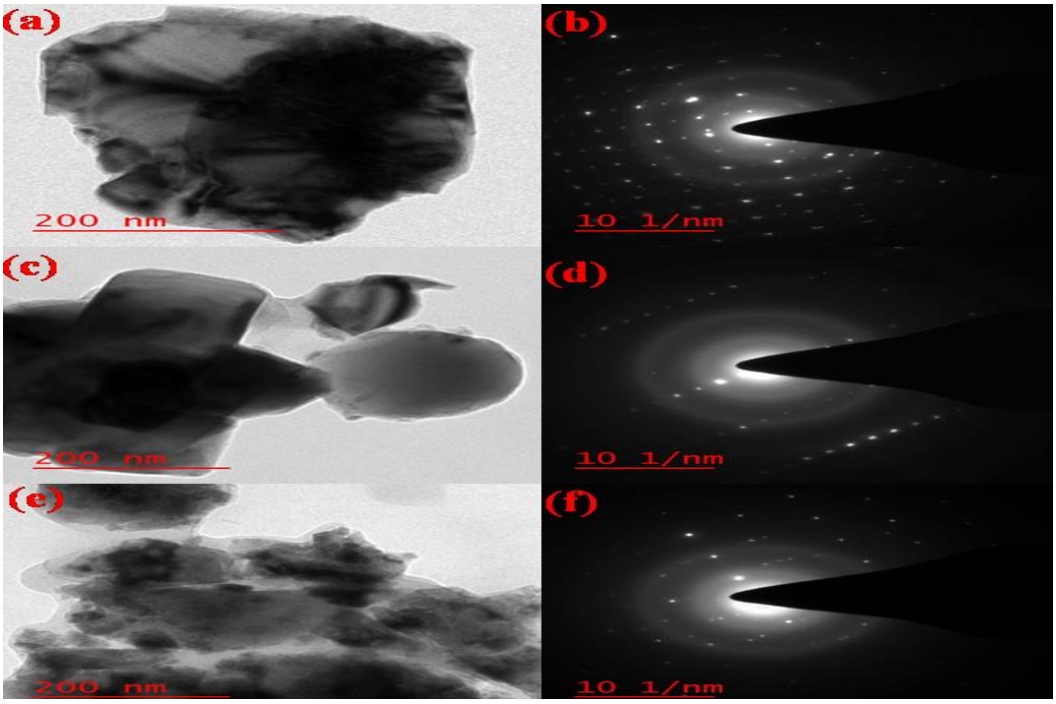

Fig. 6.2. Bright-field TEM images and their corresponding SEAD patterns of $CaCu_3Ti_{3.5}X_{0.5}O_{12}$ ceramics (a-b) X= Mn (c-d) X= Nb (e-f) X= W (Mn, Nb and W) sintered at 1223 K, 1323 K and 1373 K, respectively for 8 h.

Fig. 6.3(a-c) illustrates the SEM micrograph of CCTMO, CCTNO, and CCTWO samples, respectively. The doping of different metal ion directly affects the microstructure [18,21-24,31].CCTMO, CCTNO and CCTWO average grain size are 1.57 μm, 1.47 μm, and 1. 16 μm, respectively. The grain size directly depends on the doped or substituted metal ion. Figure 3(d-f) shows the CCTMO, CCTNO, and CCTWO energy-dispersive X-spectra (EDX) ceramics, which confirms the presence of Ca, Cu, Ti, Mn, Nb, W and O elements. Table 6.1 shows the atomic percentage of Ca, Cu, Mn, Nb, W and Ti, and

O elements with different metal ions which confirm the stoichiometry and purity of CCTMO, CCTNO, and CCTWO, respectively, ceramic materials.

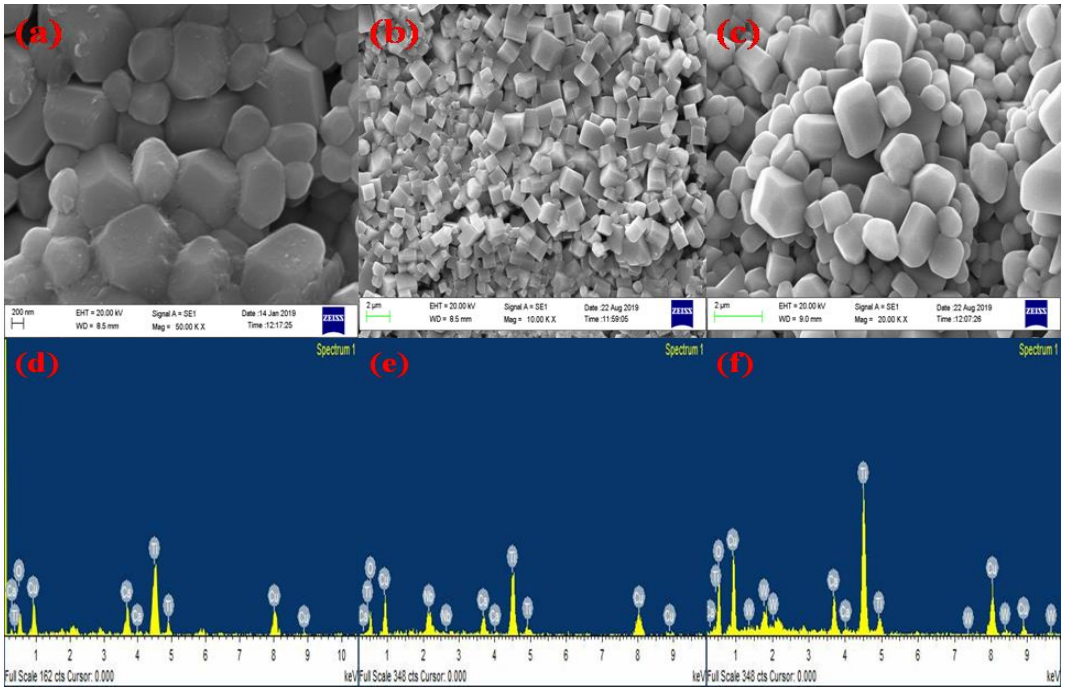

Fig. 6.3. SEM micrograph of $CaCu_3Ti_{3.5}X_{0.5}O_{12}$ ceramics (a) X= Mn (b) X= Nb (c) X= W and EDX spectra of $CaCu_3Ti_{3.5}X_{0.5}O_{12}$ ceramics (d) X= Mn (e) X= Nb (f) X= W sintered at 1223 K 1323 K and 1373 K, respectively for 8 h.

Fig. 6.4(a) presents the XPS spectrum in Mn 2p core levels for CCTMO samples sintered at 950ºC for 8 h. The highest peak at 643, 648, and 653 eV that against Mn $2p_{3/2}$ and Mn $2p_{1/2,}$ respectively shown in figure 4(a). The splitting of peak Mn 2p into Mn $2p_{3/2}$ and Mn $2p_{1/2}$ occur due to the spin-spin orbital coupling. The shoulder occurred at higher energy is show along the broadness of the peak for Mn $2p_{3/2}$ and Mn $2p_{1/2}$ as indicated by arrows which means that there are contributions from the mixed valent state of Mn ions. Due to this reason, Mn $2p_{3/2}$ and Mn $2p_{1/2}$ can further split into two other peaks by each. The deconvoluted peak of Mn $3p_{3/2}$ at 641.2 eV and 642.6 eV

(Mn $2p_{1/2}$ at 653 and 655 eV) represents the Mn^{3+} as well as Mn^{4+}, respectively [29]. This data is confirming the Mn present in both +3 and +4 oxidation states.

Fig. 6.4(b) presents the XPS spectrum in Nb 3d core levels for CCTNO ceramic sintered at 1050°C for 8 h. The highest peak at 202.7 and 202.8 eV of Nb $3d_{5/2}$ (Nb $3d_{3/2}$ at 210.2 eV) represents the Nb^{2+}, Nb^{4+} and Nb^{5+}, respectively. Fig. 4(c) shows the XPS spectrum of W 4f core levels for CCTWO at 1100°C for 8h. The main peak 34.9 and 35.2 eV of W $4f_{7/2}$ (W $4f_{5/2}$ at 37.1 and 37.4) represents the W^{4+} and W^{6+}, respectively [30]. The results of Fig 4(b & c) confirmed the oxidation state niobium and tungsten, respectively.

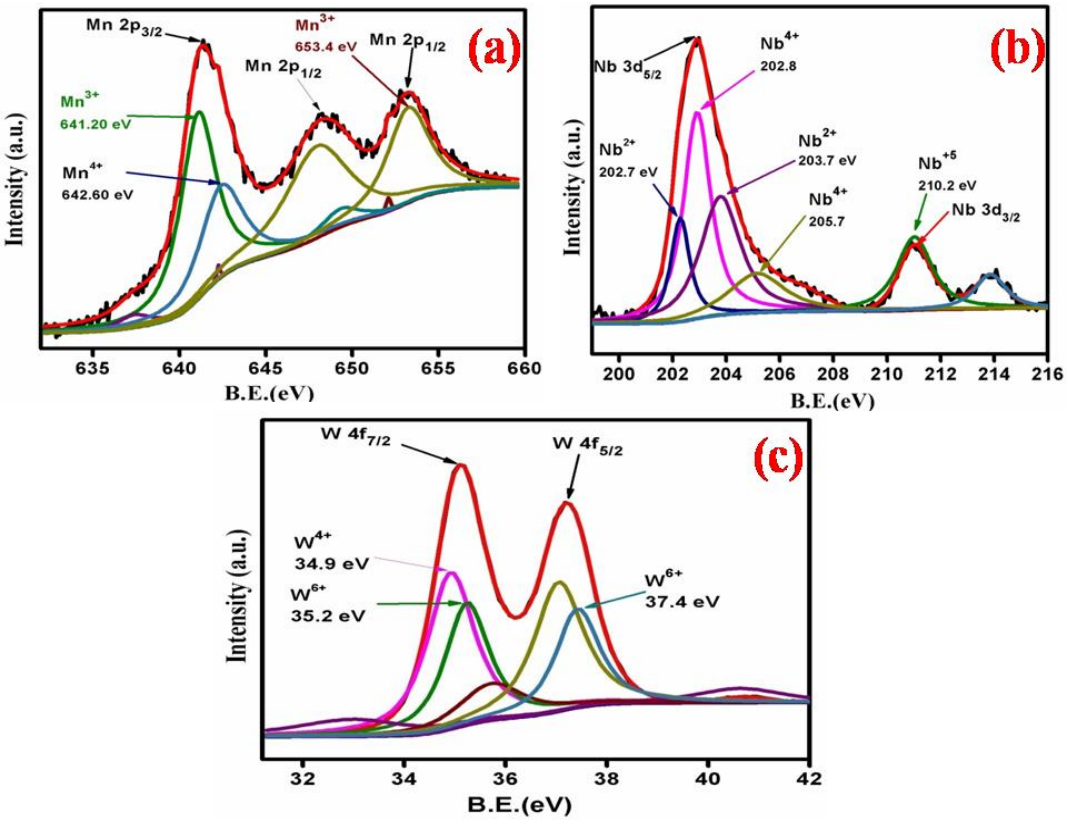

Fig. 6.4. X-ray photo emission spectroscopy (a) Mn 2p, (b) Nb 3d, (c) W 4f, for CCTXO (X= Mn, Nb, W) sintered at 1223 K, 1323 K and 1373 K, respectively for 8 h.

6.3.3 Dielectric studies

In dielectric studies, The CCTO's dielectic function value will be given to compare metal effect. Fig. 6.5(a), 6.6(a), and 6.7(a) illustrate the frequency against dielectric function (εr) at a few selected temperatures of CCTMO, CCTNO, and CCTWO, respectively. The dielectric function (εr) decreases with increasing temperature [6, 25]. The declining behavior of the dielectric function is explained by the Maxwell Wagner equation [2, 26]. In this present work, the dielectric function of both fine and abnormal grain sizes of CCTMO, CCTNO and CCTWO present the dependent frequency in the range of 100 Hz to 1 MHz The abnormal grains size of Mn, Nb and W doped-CCTO produced fine grains (show in fig.6.3 (a-c)) [27, 28]. The dielectric function (εr) of CCTMO, CCTNO, and CCTWO were found to be 800, 600, and 1500 at room temperature (308 K). The dielectric function is occurring to decrease with increasing frequency. Some literature [28] confirms the Nb-doped dielectric function is greater than CCTO. So, all this dopant can be used for refining the dielectrical behavior of CCTO. Many researchers have been investigated that the dielectric constant of the lesser substituted of a metal ion is higher in comparison to a higher substitute of metal ion CCTO [21-27, 28]. Fig. 6.5(b), 6.6(b) and 6.7(b) show the variation dielectric loss (tan δ) from 100 Hz to 1 MHz of CCTMO, CCTNO, and CCTWO at 35^{o}C. At a higher frequency region, the tangent loss decreases in all doped metal ion in CCTO. At higher frequency, the tangent loss of CCTMO, CCTNO, and CCTWO was found to be less than 1 at all selected temperature. The introduction of the doped metal ion in CCTO can exponentially decrease the dielectric constant 3 to 0.5. The result confirms that important role to decreases in dielectric loss of CCTO.

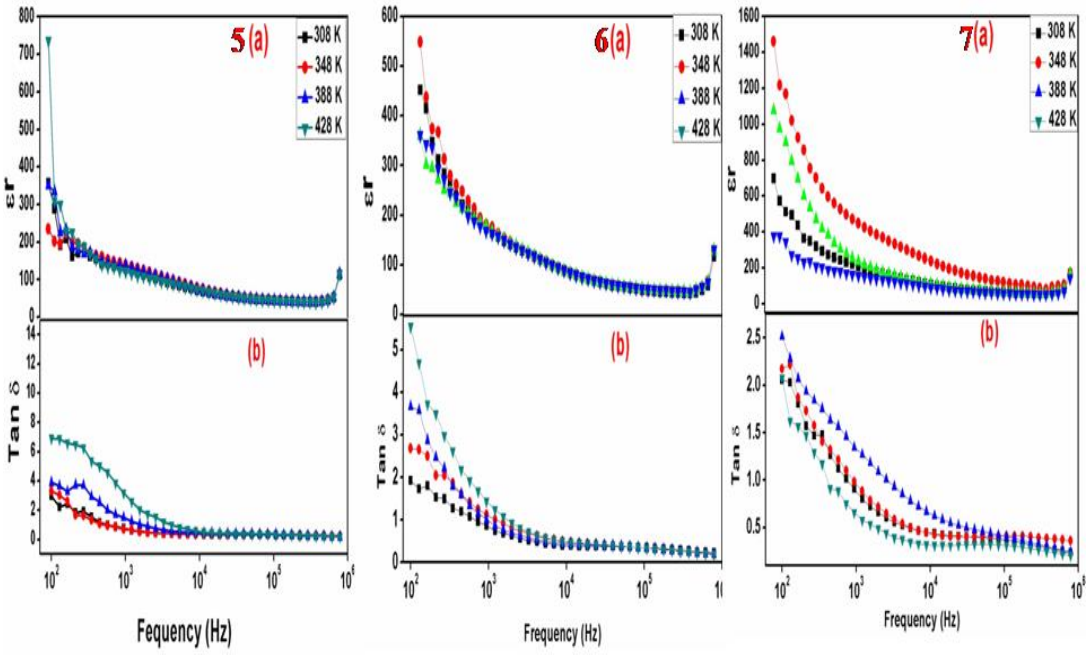

Fig. 6.5(a). Dielectric constant (b) dielectric loss dependent on the frequency at a few selected temperatures of CCTMO sintered at 1223 K for 8h.

Fig. 6.6(a). Dielectric constant (b) dielectric loss dependent on the frequency at a few selected temperatures of CCTNO sintered at 1323 K for 8h.

Fig. 6.7(a). Dielectric constant (b) dielectric loss dependent of frequency at a few selected temperatures of CCTWO sintered at 1373 K for 8h.

Conclusion

In this present work, the influence of microstructure and dielectric function of Mn, Nb, and W doped $CaCu_3Ti_4O_{12}$ (CCTO). The metal doped $CaCu_3Ti_4O_{12}$ is successfully synthesized by a semi-wet method using Metal nitrates, WO_2, Nb_2O_5 and TiO_2 in a stoichiometric amount in molar ratio as starting materials. The phase formation of CCTXO is confirmed by X-ray diffraction pattern sintered at different temperatures and indicates the presence of CCTO as the main phase containing minor phases of TiO_2.

The average crystallite size of CCTMO, CCTWO, and CCTNO was calculated 37.87 ± 10 nm, 56.23 ± 10 nm, and 42.41 ± 10 nm by XRD. The particle size of CCTXO (x= Mn, Nb, and W) occurred to be 44 nm, 101 nm, and 51 nm. The dielectric behaviors are directly affected by dopant metal ion in CCTO samples. The dielectric constant is directly dependent on grain size.

[1] Wang, T., Jin, L., Li, C., Hu, Q., & Wei, X. (2015). Relaxor ferroelectric $BaTiO_3$–$Bi(Mg_{2/3}Nb_{1/3})O_3$ ceramics for energy storage application. *Journal of the American Ceramic Society*, **98**(2), 559-566.

[2] Pandey, S., Kumar, A., Singh, N. B., & Mandal, K. D. (2020). Studies on dielectric and magnetic properties of $CaCu_3Ti_3MnO_{12}$ ceramic synthesized via semi-wet route. *Journal of the Australian Ceramic Society*, **56**(3), 915-922.

[3] Singh, L., Rai, U. S., Mandal, K. D., & Singh, N. B. (2014). Progress in the growth of $CaCu_3Ti_3MnO_{12}$ and related functional dielectric perovskites. *Progress in crystal growth and characterization of Materials*, **60**(2), 15-62.

[4] Zheng, Q., Fan, H., & Long, C. (2012). Microstructures and electrical responses of pure and chromium-doped $CaCu_3Ti_3MnO_{12}$ ceramics. *Journal of alloys and compounds*, **511**(1), 90-94.

[5] De la Rubia, M. A., Leret, P., Del Campo, A., Alonso, R. E., López-Garcia, A. R., Fernández, J. F., & De Frutos, J. (2012). Dielectric behaviour of Hf-doped $CaCu_3Ti_3MnO_{12}$ ceramics obtained by conventional synthesis and reactive sintering. *Journal of the European Ceramic Society*, **32**(8), 1691-1699.

[6] Thongbai, P., Jumpatam, J., Yamwong, T., & Maensiri, S. (2012). Effects of Ta^{5+} doping on microstructure evolution, dielectric properties and electrical response in $CaCu_3Ti_3MnO_{12}$ ceramics. *Journal of the European Ceramic Society*, **32**(10), 2423-2430.

[7] Liu, Y., Chen, Q., & Zhao, X. (2014). Dielectric response of Sb-doped $CaCu_3Ti_3MnO_{12}$ ceramics. *Journal of Materials Science: Materials in Electronics*, **25**(3), 1547-1552.

[8] Sulaiman, M. A., Hutagalung, S. D., Ain, M. F., & Ahmad, Z. A. (2010). Dielectric properties of Nb-doped $CaCu_3Ti_3MnO_{12}$ electroceramics measured at high frequencies. *Journal of alloys and compounds*, **493**(1-2), 486-492.

[9] Barbier, B., Combettes, C., Guillemet-Fritsch, S., Chartier, T., Rossignol, F., Rumeau, A., & Dutarde, E. (2009). $CaCu_3Ti_3MnO_{12}$ ceramics from co-precipitation method: Dielectric properties of pellets and thick films. *Journal of the European Ceramic Society*, **29**(4), 731-735.

[10] Masingboon, C., Thongbai, P., Maensiri, S., Yamwong, T., & Seraphin, S. (2008). Synthesis and giant dielectric behavior of $CaCu_3Ti_3MnO_{12}$ ceramics prepared by polymerized complex method. *Materials Chemistry and Physics*, **109**(2-3), 262-270.

[11] Singh, L., Rai, U. S., Rai, A. K., & Mandal, K. D. (2013). Sintering effects on dielectric properties of Zn-doped $CaCu_3Ti_3MnO_{12}$ ceramic synthesized by modified sol-gel route. *Electronic Materials Letters*, **9**(1), 107-113.

[12] Mu, C., Zhang, H., He, Y., Shen, J., & Liu, P. (2009). Influence of dc bias on the dielectric relaxation in Fe-substituted $CaCu_3Ti_3MnO_{12}$ ceramics: grain boundary and surface effects. *Journal of Physics D: Applied Physics*, **42**(17), 175410.

[13] Senda, S., Rhouma, S., Torkani, E., Megriche, A., & Autret, C. (2017). Effect of nickel substitution on electrical and microstructural properties of $CaCu_3Ti_3MnO_{12}$ ceramic. *Journal of Alloys and Compounds*, **698**, 152-158.

[14] Thongbai, P., Jumpatam, J., Yamwong, T., & Maensiri, S. (2012). Effects of Ta^{5+} doping on microstructure evolution, dielectric properties and electrical response in $CaCu_3Ti_3MnO_{12}$ ceramics. *Journal of the European Ceramic Society*, **32**(10), 2423-2430.

[15] Rai, A. K., Singh, N. K., Acharya, S. K., Singh, L., & Mandal, K. D. (2012). Effect of tantalum substitutions on microstructures and dielectric properties of calcium copper titanate ($CaCu_3Ti_3MnO_{12}$) ceramic. *Materials Science and Engineering: B*, **177**(14), 1213-1218.

[16] Lin, Y. H., Deng, W., Xu, W., Liu, Y., Chen, D., Zhang, X., & Nan, C. W. (2012). Abnormal dielectric behaviors in Mn-doped $CaCu_3Ti_3MnO_{12}$ ceramics and their response mechanism. *Materials Science and Engineering: B*, **177**(20), 1773-1776.

[17] Cai, J., Lin, Y. H., Cheng, B., Nan, C. W., He, J., Wu, Y., & Chen, X. (2007). Dielectric and nonlinear electrical behaviors observed in Mn-doped $CaCu_3Ti_3MnO_{12}$ ceramic. *Applied Physics Letters*, **91**(25), 252905.

[18] Pandey, S., & Mandal, K. D. (2019). Investigation of microstructure, ferroelectric and dielectric behavior of $CaCu_3Ti_{(4-x)}Mn_xO_{12}$ perovskites synthesized through semi-wet route. *SN Applied Sciences*, **1**(12), 1-7.

[19] Lin, Y. H., Cai, J., Li, M., Nan, C. W., & He, J. (2006). High dielectric and nonlinear electrical behaviors in Ti O 2-rich $CaCu_3Ti_3MnO_{12}$ ceramics. *Applied Physics Letters*, **88**(17), 172902.

[20] Mandal, K. D., Rai, A. K., Kumar, D., & Parkash, O. (2009). Dielectric properties of the $Ca_{1-x}LaxCu_3Ti_{4-x}Co_xO_{12}$ system (x= 0.10, 0.20 and 0.30) synthesized by semi-wet route. *Journal of alloys and compounds*, **478**(1-2), 771-776.

[21] Singh, L., Sin, B. C., Kim, I. W., Mandal, K. D., Chung, H., & Lee, Y. (2016). A novel one-step flame synthesis method for tungsten-doped CCTO. *Journal of the American Ceramic Society*, **99**(1), 27-34.

[22] Sulaiman, M. A., Hutagalung, S. D., Ain, M. F., & Ahmad, Z. A. (2010). Dielectric properties of Nb-doped $CaCu_3Ti_3MnO_{12}$ electroceramics measured at high frequencies. *Journal of alloys and compounds*, **493**(1-2), 486-492.

[23] Zheng, Q., Fan, H., & Long, C. (2012). Microstructures and electrical responses of pure and chromium-doped $CaCu_3Ti_3MnO_{12}$ ceramics. *Journal of alloys and compounds*, **511**(1), 90-94.

[24] Senda, S., Rhouma, S., Torkani, E., Megriche, A., & Autret, C. (2017). Effect of nickel substitution on electrical and microstructural properties of $CaCu_3Ti_3MnO_{12}$ ceramic. *Journal of Alloys and Compounds*, **698**, 152-158.

[25] Thongbai, P., Jumpatam, J., Putasaeng, B., Yamwong, T., & Maensiri, S. (2012). The origin of giant dielectric relaxation and electrical responses of grains and grain boundaries of W-doped $CaCu_3Ti_3MnO_{12}$ ceramics. *Journal of Applied Physics*, **112**(11), 114115.

[26] George, M., Nair, S. S., Malini, K. A., Joy, P. A., & Anantharaman, M. R. (2007). Finite size effects on the electrical properties of sol–gel synthesized $CoFe_2O_4$ powders: deviation from Maxwell–Wagner theory and evidence of surface polarization effects. *Journal of Physics D: Applied Physics*, **40**(6), 1593.

[27] Sulaiman, M. A., Hutagalung, S. D., Mohamed, J. J., Ahmad, Z. A., Ain, M. F., & Ismail, B. (2011). High frequency response to the impedance complex properties of Nb-doped $CaCu_3Ti_3MnO_{12}$ electroceramics. *Journal of Alloys and Compounds*, **509**(18), 5701-5707.

[28] Sulaiman, M. A., Hutagalung, S. D., Ain, M. F., & Ahmad, Z. A. (2010). Dielectric properties of Nb-doped $CaCu_3Ti_3MnO_{12}$ electroceramics measured at high frequencies. *Journal of alloys and compounds*, **493**(1-2), 486-492.

[29] Sannigrahi, J., Chattopadhyay, S., Dutta, D., Giri, S., & Majumdar, S. (2013). Magnetic and electric properties of $CaMn_7O_{12}$ based multiferroic compounds: effect of electron doping. *Journal of Physics: Condensed Matter*, **25**(24), 246001.

[30] Singh, L., Sin, B. C., Kim, I. W., Mandal, K. D., Chung, H., & Lee, Y. (2016). A novel one-step flame synthesis method for tungsten-doped CCTO. *Journal of the American Ceramic Society*, **99**(1), 27-34.

[31] Pandey, S., Kumar, V., & Mandal, K. D. (2020). Studies of sintering temperature on the microstructure, magnetic and dielectric behavior of $CaCu_3Ti_{3.5}Mn_{0.5}O_{12}$ ceramic synthesized by semi-wet route. *SN Applied Sciences*, **2**(3), 1-9.

Summary

- $CaCu_3Ti_4O_{12}$ (CCTO) ceramic was synthesized by semi-wet route at low temperature and single phase formation was confirmed by XRD studies.
- The elemental compositions of Mn-doped CCTO ceramics obtained by EDX data were fit as per stoichiometric ratio of the elements in both the ceramics.
- Dielectric constant of Mn-doped CCTO ceramic was found lower than CCTO ceramic at all measured temperature and frequency.
- The blocking temperature of CCTO and doped CCTO ceramics obtained by magnetic measurement was found to be 25 K and 155 K, respectively.
- The dielectric constant of Mn-doped composites were found to be 100 to 1200 at 303, 363, and 423 K and 484 K, at 100 Hz. the dielectric constant is highest in the case of low concentration of Mn doped CCTO.
- The Neel's temperature obtained by magnetic measurement was found to be 25 K for all the synthesized composite.

Future Scope

In general, this work has been important for nature. The everyday increasing demand for various applications, semiconducting technology sustain blest in its drive for high transistor densities and faster transistor.

Ceramic has inorganic and non-metallic materials constituted from metal and a non metal compounds. New days ceramic materials have enormously expanded many possible applications. Most of the new materials have used in our daily life. There is now a strong researcher effort to discover the new ceramics and their composites for various applications. Composite have played an important role in industrial application. Composites have constituted penetration into devices end-use segments and the development efforts newer composition for existing and novel application.

- The calcium copper titanium oxides ($C_aCu_3Ti_4O_{12}$) may be used in various applications because of its high dielectric constant and low coercivity value.
- The $CaCu_3Ti_3MnO_{12}$ ceramics shows great interested in ferroelectric materials for its application in non-volatile random access memories (NRAM) and advanced MOS transistors.
- The composite materials of CCTO and BCTO shows enhanced properties as compared to its parents components and may be used in capacitors, microelectronic devices and electronic chips, transistors.
- The composite materials show soft as well as hard magnetic nature due to different composition of parent compound which are suitable for computer chips, transformer, hard disk and floppy disk.
- The properties of ceramics and composite largely depend on the synthesis route, sintering duration and sintering temperature. In future, these composite may be

studied by changing the synthesis route and sintering condition.

- The internal properties of the composite may be studied by impedance analysis to see the electrical and dielectrical properties of grain and grain boundries.
- Electrical polarization of the composite may be studied with variation of temperature by P-E loop tracer.

List of Publications

1. Santosh Pandey, Atendra Kumar, N. B. Singh, and K. D. Mandal. *Journal of the Australian Ceramic Society* (2019): 1-8.

2. Santosh Pandey, and K. D. Mandal. *SN Applied Sciences* 1, no. 12 (2019): 1738.

3. Santosh Pandey, Vinod Kumar, and K. D. Mandal. *SN Applied Sciences* 2, no. 3 (2020): 1-9.

4. Santosh Pandey, Vinod Kumar, Vinay Kumar Sharma, and K. D. Mandal. *Materials Chemistry and Physics* (2020): 123384.

5. Kumar, Vinod, Atendra Kumar, Manish Kumar Verma, Shruti Singh, **Santosh Pandey**, Vishnu Shankar Rai, Dinesh Prajapati, Tapas Das, N. B. Singh, and K. D. Mandal. *Materials Chemistry and Physics* 245 (2020): 122804.

6. Kumar, Vinod, Atendra Kumar, Manish Kumar Verma, Shruti Singh, **Santosh Pandey**, Laxman Singh, N. B. Singh, and K. D. Mandal. *Arabian Journal of Chemistry* (2020).

7. Kumar, Vinod, **Santosh Pandey,** Shruti Singh, Manish Kumar Verma, Atendra Kumar, N. B. Singh, and K. D. Mandal. *Journal of the Australian Ceramic Society* (2020): 1-7.

8. Kumar, Vinod, **Santosh Pandey**, Atendra Kumar, Manish Kumar Verma, Shruti Singh, Vishnu Shankar Rai, Dinesh Prajapati and K.D Mandal. *Journal of Materials Research and Technology* 9, no. 6 (2020): 12936-12945.

9. Vishnu Shankar Rai, **Santosh Pandey**, Vinod Kumar, Manish Kumar Verma, Atendra Kumar, Shruti Singh, Dinesh Prajapati, and K. D. Mandal. *J Mater Sci: Mater Electron* (2021).